Synthesis of Ag–In binary sulfide nanoparticles—structural tuning and their photoluminescence properties

Tetsuya Ogawa,[a] Toshihiro Kuzuya,*[b] Yasushi Hamanaka[a] and Kenji Sumiyama[a]

Received 6th October 2009, Accepted 17th December 2009
First published as an Advance Article on the web 2nd February 2010
DOI: 10.1039/b920732e

In this report, we demonstrate the synthesis of binary sulfide Ag–In–S NPs using a Ag–In thiolate complex. Thermal decomposition of the thiolate complex provides $Ag/AgInS_2$ heterostructured nanoparticles (NPs). A metathesis reaction between the thiolate complex and sulfur source leads to the formation of nearly monodispersed $AgInS_2$ NPs with a chalcopyrite-like or orthorhombic structure. $AgInS_2$ NPs with a chalcopyrite-like structure exhibited room temperature photoluminescence (PL). Spectral shift of the PL band depending on the excitation laser intensity and characteristic behavior of the PL decay time varying over a wide energy range within the PL band were observed. These results indicate that the PL of the $AgInS_2$ NPs may be attributed to the donor–acceptor (D–A) pair recombination.

1. Introduction

I-III-VI_2 ($AgMX_2$, $CuMX_2$; M = Al, Ga, In; X = S, Se) and related materials are considered to be the most promising candidates as substitutes for II-VI semiconductor nanoparticles (NPs). $CuInS_2$ (CIS) with a chalcopyrite structure has a large absorption coefficient (CIS: $\sim 10^5$ cm^{-1}), a large tolerance for cosmic rays and an optimum band gap ($\sim$1.5eV) for a photovoltaic cell. CIS thin films are suitable for absorber layers of hetero-junction solar cells.[1] Indeed, Honda Motor Co. and Showa Shell Sekiyu K.K. started to mass produce I-III-VI_2 solar cells with quantum efficiency $>\sim$12% in 2007.[2] On the other hand, Guo *et al.* and Korgel *et al.* demonstrated low cost $CuInSe_2$ (CISe) thin film fabrication by using a CISe NPs ink spin coat technique.[3] Schoonman *et al.* fabricated a TiO_2–CIS NP composite film, and demonstrated that this composite film served as a photovoltaic cell with 4% conversion efficiency[1e]. Also, several reports demonstrated the room temperature photoluminescence (PL) of I-III-VI_2 NPs, which were synthesized *via* thermolysis of $(PPh_3)_2CuIn(SEt)_4$,[4a] $(PPh_3)_2AgIn(SeC\{O\}Ph)_4$,[4b] and dithiocarbamate[5] and –thiolate[6a,b]. PL quantum efficiencies of these I-III-VI_2 NPs attained 5–20%. On the other hand, Tian *et al.*[7] and Hamanaka *et al.*[8] reported the large nonlinear optical properties of $AgInS_2$(AIS) and CIS NPs comparable to the II-VI semiconductor NPs. These attractive linear and nonlinear optical properties encouraged us to finely investigate I-III-VI_2 NPs' properties and to develop a novel synthesis route associated with low cost and large scale production.

In the above mentioned investigations, various processes have been used to successfully synthesize various chalcopyrite NPs. Though fabrication of metal/semiconductor heterostructured NPs and control of the crystalline structure are required to develop nano-size components for energy devices, there are few reports dealing with these problems. In this report, the syntheses of $AgInS_2$ NPs were conducted by thermolysis of Ag–In thiolate, and metathesis reactions between a metal thiolate and a sulfur source, in which the fabrication of $Ag/AgInS_2$ heterostructured NPs and the control of the crystalline structure (chalcopyrite-like or orthorhombic) were achieved. These results indicated the general strategy for a synthesis of binary chalcogenide NPs with a heterostructure and a metastable crystalline structure.

$AgInS_2$ NPs with small size dispersions have been synthesized and examined with PL spectroscopy in conjunction with time-resolved PL measurements. PL spectra indicate that $AgInS_2$ NPs exhibit a broad PL band with large Stokes shifts at room temperature. We have observed that the spectral shift of the PL band is dependent upon the excitation laser intensity, and characteristic behavior of the PL decay time varies over a wide energy range within the PL band. The results indicate that the PL of the $AgInS_2$ NPs can be attributed to the donor–acceptor (D–A) pair recombination. To our best knowledge, this is the first report dealing with a detailed PL mechanism of Ag–In–S NPs.

2. Experimental procedures

2.1 Synthesis process

The typical experimental procedures for the synthesis of $AgInS_2$ NPs are described as follows: all reagents are used as received. **Ag-In thiolate solution:** 0.4 mmol of silver(I) acetate (Ag(ace)) and indium(III) acetate ($In(ace)_3$) are mixed with 1-dodecanethiol (DT) solution in a round-bottom flask, which is degassed by Ar gas flushing for 2 h at 423 K. **The case of thermal decomposition of thiolate:** After the addition of tri-*n*-octylamine (TOCA) into Ag-In thiolate solution and Ar-flushing, the mixture solution is heated up to 483–543 K for 2 h. **The case of metathesis reaction between metal thiolate and sulfur source:** 5 ml of sulfur ligand (DT or alkyl amine) solution, in which 26.2 or 104.8 mg (0.8 S × 1 or 3.2 S × 4) of sulfur powder is dissolved, is rapidly injected into the Ag-In thiolate solution and heated up to 423–543 K for 2 h.

[a]*Department of Materials Science and Engineering, Nagoya Institute of Technology, Japan*
[b]*Department of Materials Science and Technology, Muroran Institute of Technology, 27-1 Mizumoto-cho, Muroran, Hokkaido, 050-8585, Japan. E-mail: kuzuya@mmm.muroran-it.ac.jp; Fax: +81-143-46-5639; Tel: +81-143-46-5639*

Table 1 Experimental conditions

Sample name	Ag(ace)/mg	$In(ace)_3$/mg	DT/ml	S/mg	Alkyl amine[a]/g	Reaction temperature/K	Appeared in
SA1	67.4	116.8	2.46	—	16.2 (TOCA)	493	Fig. 1(a),(b), Fig. 2(a)
SA2	67.4	116.8	15	26.2	2.15 (DA)	513	Fig. 1(c), Fig. 2(b), Fig. 3
SA3	67.4	116.8	17.6	26.2	—	423	Fig. 1(d) upper, Fig. 2(c)
SA4	67.4	116.8	17.6	104.8	—	423	Fig. 1(d) lower, Fig. 2(d), Fig. 3–5
SA5	67.4	116.8	17.6	26.2	—	513	Fig. 1(e), Fig. 2(e), Fig. 3
SA6	67.4	116.8	17.6	26.2	—	543	Fig. 1(f), Fig. 2(f), Fig. 3

[a] DA: Dodecylamine, TOCA: Tri-*n*-octyl amine.

Experimental conditions are summarized in Table 1. **Recovery of NPs:** After the solution has cooled to room temperature, ethanol is added and precipitates are obtained. They are separated by centrifugation to remove excess reagents and then redispersed in hexane. This precipitate–redispersion procedure is repeated several times to purify the precipitates.

2.2 Characterizations

2.2.1 TEM and XRD. For transmission electron microscope (TEM) observation, a drop of $AgInS_2$ colloidal solution is placed onto a carbon-coated TEM grid and examined with a Hitachi HF-2000 field emission TEM operating at 200 kV with a resolution of 0.23 nm. The crystal structures of $AgInS_2$ NPs are identified by X-ray diffraction (XRD, Mac Science, M18XCE) using sol samples dried onto glass plates.

2.2.2 Optical spectroscopy. The optical properties of $AgInS_2$ NPs prepared by the metathesis reaction are studied by UV-Vis and PL spectroscopy. UV-Vis absorption spectra are measured in the wavelength range between 200 and 1200 nm using a double-beam spectrophotometer (JASCO V-570). PL spectra are measured by a spectrograph equipped with a cooled CCD detector. A 532 nm (2.33 eV) line of a continuous-wave diode laser is used as the excitation source. The calibration of the relative spectral sensitivity of the PL spectrometer is done by comparing a fluorescence spectrum of 4-dimethylamino-4′-nitrostilbene–*o*-dichlorbenzol solution measured by our system to its standard spectrum.[9] In PL decay time measurements, the sample is excited by a pulsed dye laser (repetition rate: 10 Hz, pulse duration: 10 ns) and the detection energy was selected by a monochromator. PL decay curves at the selected energies are recorded by a photomultiplier tube and a digital oscilloscope. All spectral measurements are carried out for a colloidal solution of $AgInS_2$ NPs in hexane at room temperature.

3. Results

3.1 Synthesis

Fig. 1(a)–(f) show TEM images of Ag–In–S NPs obtained by the thermolysis of Ag–In thiolate and metathesis reactions. The thermolysis of thiolate leads to the formation of irregular shape NPs, shown in Fig. 1(a) and (b). The high resolution TEM image (Fig. 1(b)) reveals that the dendrite-like crystals grow on a core NP with a polyhedral shape (arrow in Fig. 1(b)). Fig. 1(c)–(f) show the Ag–In–S NPs obtained by the metathesis reaction between Ag–In thiolate and various sulfur sources: Fig. 1(c) for S-dodecylamine (S-DA) and Fig. 1(d)–(f) for S-dodecanethiol (S-DT). Fig. 1(c) reveals that the metathesis reaction between Ag–In thiolate and S-DA provides NPs with relatively low polydispersity and 5.6 ± 1.1 nm average diameter. Compared with S-DA, the average size of NPs obtained by using S-DT is

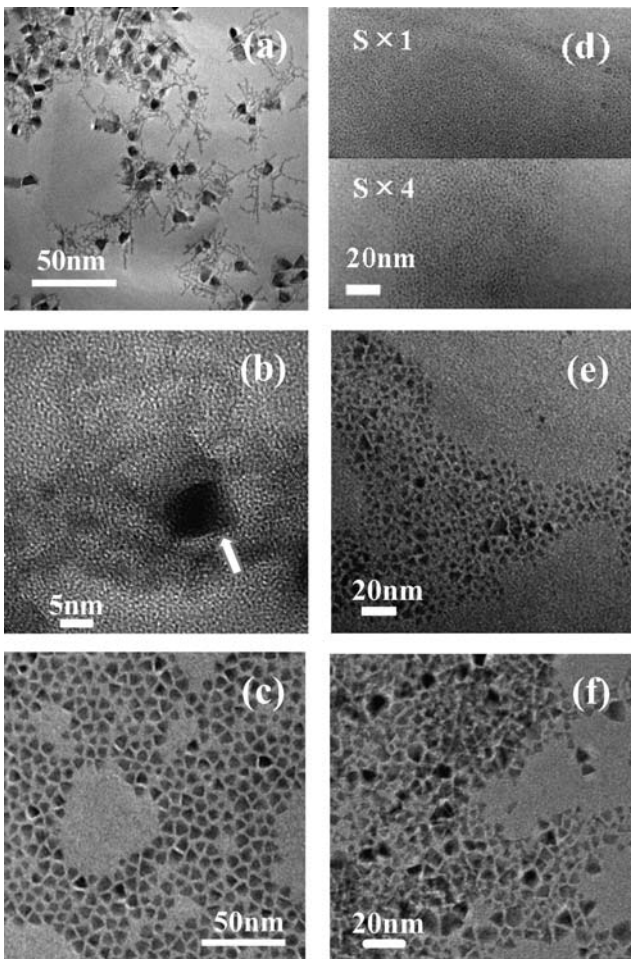

Fig. 1 TEM images of $AgInS_2$ NPs obtained under various experimental conditions. (a) Ag/$AgInS_2$ composite NPs synthesized *via* thermolysis of Ag–In thiolate, (b) high resolution TEM image of Ag/$AgInS_2$ composite NPs, (c)–(f) $AgInS_2$ NPs synthesized *via* the metathesis reaction. Using S-DA: (c) 513 K (S × 1). Using S-DT: (d, upper) 423 K (S × 1), (d, lower) 423 K (S × 4), (e) 513 K (S × 1), and (f) 543 K (S × 1). The arrow in (b) indicates the Ag core NP.

relatively small. TEM images of NPs synthesized using S-DT at various sulfur concentrations and reaction temperatures are shown in Fig. 1(d)–(f), (d, upper) 423 K (S × 1), (d, lower) 423 K (S × 4), (e) 513 K (S × 1) and (f) 543 K (S × 1), respectively. The sizes of NPs and their distributions increase with the increase in the reaction temperature. However, the effect of sulfur concentration on the NPs' size was not confirmed (see Fig. 1(d) upper (S × 1) and lower (S × 4)). In addition, the higher reaction temperature lead to the formation of NPs with a triangle shape (shown in Fig. 1(f)).

Fig. 2(a), (c), (d), (e) and (f) show the XRD patterns of the NPs obtained by the thermolysis of Ag–In thiolate (a) and the metathesis reaction between Ag–In thiolate and S-DT (c)–(f). They exhibit diffraction patterns which resemble that of $AgInS_2$ with a chalcopyrite (see Fig. 2(g)) or zinc blende structure. $AgInS_2$ with the chalcopyrite structure exhibits a diffraction peak at $2\theta = 35.04°$, which corresponds to (211). However, the (211) peak could not be detected in these XRD patterns. The relative intensity $I(211)/I(112)$ is <1, being too small to be detected. Therefore, the crystalline structure of the NPs could not be identified as either the chalcopyrite ($2a \neq c$) or zinc blende ($2a = c$; random ordering, chalcopyrite-like) structures.

In Fig. 2(a), the co-existence of a Ag metallic phase with an fcc structure is also confirmed by the characteristic peaks indicated by filled circles in Fig. 2(a). As mentioned above, NPs obtained by the thermolysis of thiolate consist of a polyhedral core and dendrite-like crystals. These results indicate that thermolysis of Ag–In thiolate provided Ag(core)–$AgInS_2$ (dendrite-like) heterostructured nanomaterials. Fig. 2(b)–(f) indicate that the sulfur source plays an important role in the polymorphism of Ag–In–S NPs. NPs obtained using the metathesis reaction between Ag–In thiolate and S-DA take an orthorhombic structure (indicated by filled triangles, JCPDS 00-025-1328). Using S-DT leads to the formation of NPs with a chalcopyrite or zinc blende structure (see Fig. 2(g)). FWHM values of NPs at various reaction temperatures, (c) 423 K (S × 1), (e) 513 K (S × 1) and (f) 543 K (S × 1), indicate that the NPs' size depends upon the reaction temperature. The average sizes of NPs estimated by the Scherrer equation are (c) 2.5, (e) 3.4 and (f) 4.3 nm respectively. On the other hand, the sulfur concentration does not affect the size of the NPs (see Fig. 2(c) and (d), 2.5 nm). These results are consistent with those obtained from the TEM images shown in Fig. 1(d)–(f).

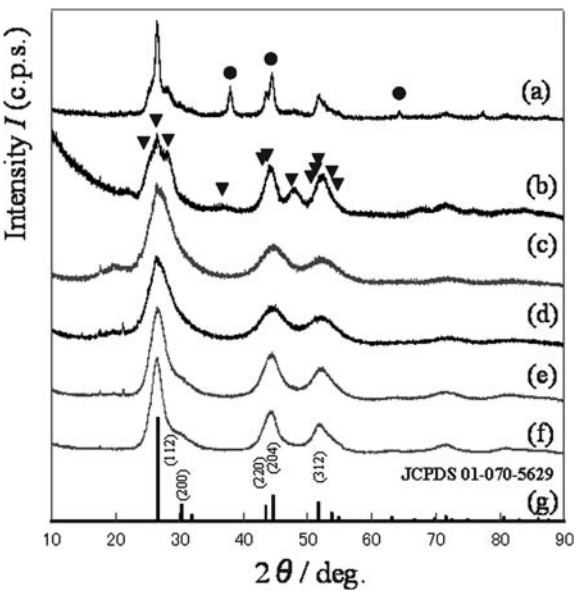

Fig. 2 XRD patterns of $AgInS_2$ NPs obtained under various experimental conditions. (a) Ag/$AgInS_2$ composite NPs synthesized *via* thermolysis of Ag–In thiolate, (b)–(e) $AgInS_2$ NPs synthesized *via* the metathesis reaction. (b) Using S-DA (S × 1) at 513 K; (c)–(e) using S-DT at: (c) 423 K (S × 1), (d) 423 K (S × 4), (e) 513 K (S × 1), (f) 543 K (S × 1); and (g) $AgInS_2$ chalcopyrite structure. Filled circles and triangles represent the peak positions of Ag with fcc structure and $AgInS_2$ with orthorhombic structure, respectively.

3.2 UV-Vis absorption and photoluminescence characteristics

Fig. 3 shows the UV-Vis absorption spectra of NPs prepared by the metathesis reaction between thiolate and the sulfur source. In the UV-Vis absorption spectra, a shoulder or broad peak around 2.2–2.6 eV is observed. We have estimated the peak positions of these absorption bands from the extrema of the corresponding second derivative spectra. Energy positions of the absorption bands are determined to be 2.61, 2.38, and 2.26 eV for NPs with diameters of 2.5 (SA4), 3.4 (SA5) and 4.3 nm (SA6) synthesized by the use of S-DT, respectively, and 2.22 eV for 5.6 nm (SA2) NPs synthesized by the use of S-DA, which are marked by the arrows and vertical dashed lines in Fig. 3.

PL spectra of $AgInS_2$ NPs with diameters of 2.5 (SA4), 3.4 (SA5) and 4.3 nm (SA6) synthesized with S-DT are shown in Fig. 3. The broad emission bands with FWHM of 370–400 meV and peak energies of 1.61, 1.51, and 1.45 eV are observed for NPs with diameters of 2.5, 3.4, and 4.3 nm, respectively. We could not measure the PL spectra below 1.2 eV due to low sensitivity of the CCD detector. In order to investigate the PL emission mechanism of $AgInS_2$ NPs, we have measured the PL spectra by varying the excitation intensity over a wide range and the PL decay time. The PL spectra of $AgInS_2$ NPs with a diameter of 2.5 nm (SA4) observed for various excitation intensities are shown in Fig. 4(a), and emission peak energies are plotted *versus* relative excitation intensity in the inset of Fig. 4(a). The results show that the PL emission energy increases from 1.594 to 1.614 eV with increasing relative excitation intensity from

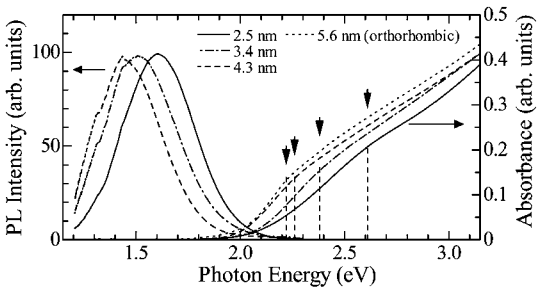

Fig. 3 UV-Vis absorption and PL spectra of $AgInS_2$ NPs synthesized using S-DT at 423 K (2.5 nm (SA4), —), 513 K (3.4 nm (SA5), ·-·-), and 543 K (4.3 nm (SA6), ---). The UV-Vis absorption spectrum of $AgInS_2$ NPs synthesized using S-DA at 513 K (5.6 nm (SA2)) is shown as a dotted curve. Down arrows indicate the position of absorption peaks or shoulders of each spectrum.

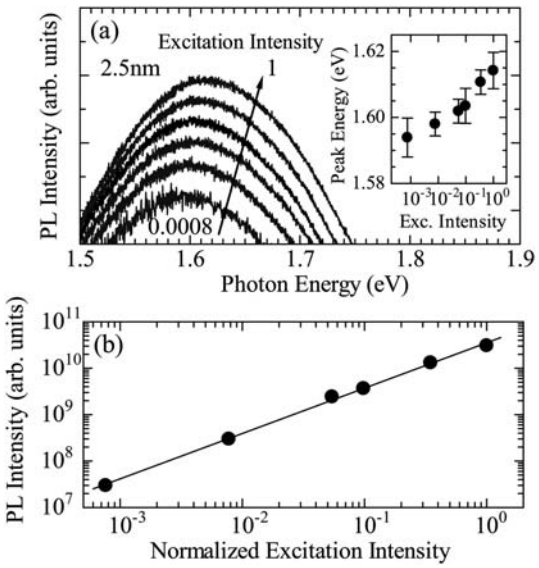

Fig. 4 (a) Excitation intensity dependence of the PL spectra of $AgInS_2$ NPs synthesized at 423 K using S-DT (2.5 nm (SA4)). The inset shows the relationship between the emission peak energy and relative excitation intensity. (b) PL intensity measured at the peak energy *vs.* relative excitation intensity. The line represents the result of the fitting analysis.

0.0008 to 1. In Fig. 4(b), the PL intensity at the emission band maximum (I) is plotted as a function of the excitation intensity (L). The experimental data can be well fitted by an $I \propto L^k$ law, and an exponent k is determined to be 0.97.[10]

PL decay profiles following a pulsed laser excitation at 2.58 eV were measured at various detection energies between 1.44 and 2.30 eV. Some of the decay curves obtained for NPs with a diameter of 2.5 nm (SA4) are shown in the inset of Fig. 5. The decay curves exhibited non-exponential features for any emission energies, so the PL decay curves were fitted by the following equation assuming the two exponential components:

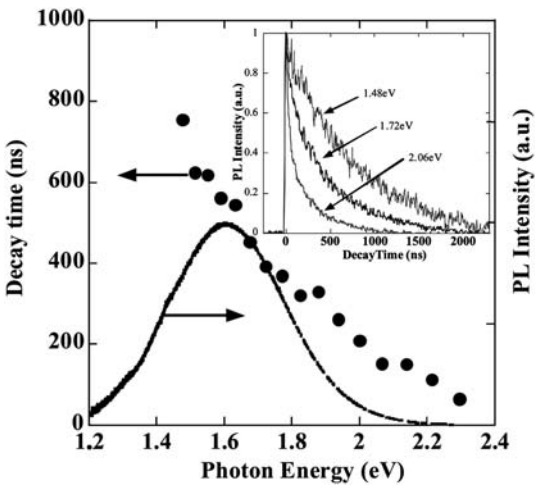

Fig. 5 The effective PL decay times of $AgInS_2$ NPs synthesized at 423 K using S-DT (D = 2.5 nm (SA4)) plotted as a function of emission energy (●) and the corresponding time-integrated PL spectrum. The inset shows the PL decay curves measured at various emission energies.

$$I(t) = A\exp\left(-\frac{t}{\tau_A}\right) + B\exp\left(-\frac{t}{\tau_B}\right) \quad (1)$$

We have estimated the PL decay time by the effective values τ^*, which are defined by:

$$\tau^* = \frac{A\tau_A + B\tau_B}{A + B} \quad (2)$$

where parameters A, B, τ_A, and τ_B were determined by fitting analysis. The results of the fitting analysis indicate that the values of τ_A and τ_B vary over a wide range depending on the detection energy. The values of τ_A and τ_B are estimated to be ~20 ns and ~200 ns, respectively, for 2.30 eV, and monotonously extend to ~130 ns and ~800 ns for 1.44 eV. Simultaneously, relative contribution ratios of the shorter and longer decay components A/B decrease from 3 for 2.30 eV to 0.1 for 1.44 eV. In Fig. 5, the effective decay times τ^* calculated using eqn (2) are plotted as a function of emission energy together with the PL spectrum of the same $AgInS_2$ NPs. The τ^* value increased from ~60 ns to ~760 ns with decreasing emission energy from 2.30 to 1.44 eV, indicating that the PL decay time depends strongly upon the emission energy, such that the decay is faster for the higher emission energy. Similar characteristic dependencies of the PL peak energy and PL intensity on the excitation intensity, and similar tendencies in the spectral variation of the PL decay time, were observed for NPs with diameters of 3.4 (SA5) and 4.3 nm (SA6) (not shown).

4. Discussion

4.1 Formation mechanism of $AgInS_2$ NPs

Metal thiolates polymerize to form a gelatinous compound, which is thermally decomposed to highly monodispersed metal sulfide NPs.[11] The thiol group serves not only as a sulfur source, but also a bridging ligand which coordinates multiple metal ions. This fact reminds us to introduce a metal thiolate mixture into a synthesis of chalcopyrite NPs. Indeed, I-III Cu–In thiolates were used as single-source precursors for syntheses of $CuInS_2$ NPs with

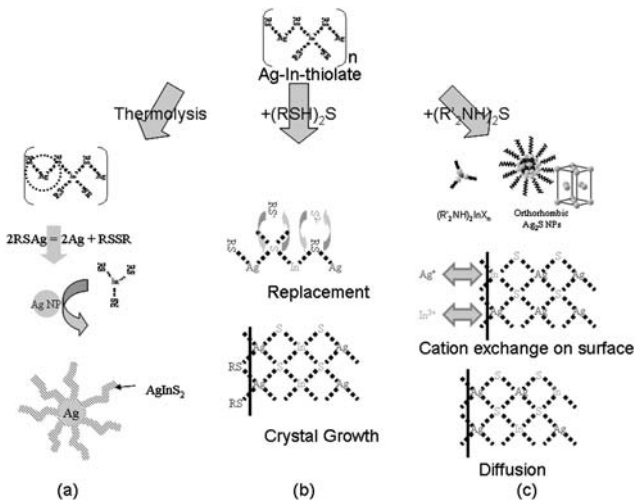

Fig. 6 Schematic illustrations of formation mechanisms. (a) Thermal decomposition of Ag–In thiolate, (b) metathesis reaction between Ag–In thiolate and $(RSH)_2S$, and (c) between Ag–In thiolate and $(R'_2NH)_2S$.

a chalcopyrite structure.[6,8] However, in the case of thermal decomposition of Ag–In thiolate, metal nuclei were generated and then grew into metal-semiconductor heterostructured NPs. Because of the electron donor nature of the thiol molecule, Ag–thiol bonds decomposed into RSSR and Ag^0 (shown in Fig. 6(a)). Then, indium sulfide species formed *via* the thermolysis of In–thiolate complexes. Ag^0 in coexistence with sulfur sources is thermodynamically unstable,[12] consequently, indium sulfide species reacted with Ag^0 to form $AgInS_2$ dendrites on the NP's surface. The detailed mechanisms are under investigation.

In order to synthesize nearly monodispersed $AgInS_2$ NPs with a homogeneous structure, the reaction between Ag–In thiolate and the sulfur source (S-DT ($(RSH)_2S$) or S-DA ($(R'_2NH)_2S$)) was selected instead of thermolysis of Ag–In thiolate. Because of the electron donor nature of the thiol and amine groups, these sulfur sources easily release H_2S or S^{2-} at room temperature.[13] The formation mechanisms are considered to be as follows: a thiol ion (RS^-) in a Ag–In bridged complex is exchanged for a S^{2-} ion to form a –Ag–S–In– unit, which polymerizes to form a Ag–In–S lattice (shown in Fig. 6(b)). However, this model cannot well explain the formation of $AgInS_2$ NPs with an orthorhombic structure. Therefore, an alternative pathway, a "cation doping process", should be taken into account to elucidate the formation pathway of $AgInS_2$ NPs with an orthorhombic structure. The cation doping process consists of the pre-formation of monosulfide NPs such as Ag_2S and In_2S_3, a cation exchange on the surface of the monosulfide NPs, and the diffusion of dopant cations (step 3)[14] (Fig. 6(c)). In this case, a binary sulfide NP ($AgInS_2$) has the same sulfur sub-lattice as the seed NP; that is, the formation of NPs with chalcopyrite-like and orthorhombic structures requires monosulfide NPs with an fcc and an orthorhombic sulfur sub-lattice, respectively. Crystalline Ag_2S is known to have a monoclinic structure at <452 K, a bcc structure at <859 K, an fcc sulfur sub-lattice (γ-Ag_2S) at >859 K[15a] and an orthorhombic sulfur sub-lattice in the nano size range at ~413 K[15b]. In_2S_3 crystals also take a defect sphalerite structure (α-In_2S_3) at >693 K, which has an fcc sulfur sub-lattice[15c]. Therefore, under our experimental conditions (<543 K), the cation doping process can provide $AgInS_2$ NPs with orthorhombic structure *via* the pre-formation of orthorhombic Ag_2S NPs. However, because the formation of fcc seed NPs (γ-Ag_2S and α-In_2S_3) is thermodynamically less favored at lower than 859 (γ-Ag_2S) and 693 K (α-In_2S_3), the cation doping process cannot explain the formation of chalcopyrite-like $AgInS_2$. Our experimental results indicate that the co-existence of aliphatic amines (such as DA, hexadecylamine, oleylamine and so on) in sulfur sources plays an important role in the formation of orthorhombic $AgInS_2$ NPs. In the case of $(RSH)_2S$, the $AgInS_2$ with chalcopyrite-like structure is formed *via* the scheme shown in Fig. 6(b). When S-DA is used as a sulfur source, the difference in the affinity of DA for metal ions may lead to the decomposition of Ag–In thiolate. Consequently, the formation of $AgInS_2$ with orthorhombic structure proceeds *via* the scheme shown in Fig. 6(c). The formation mechanism must be further examined.

4.2 Optical properties of $AgInS_2$ NPs

4.2.1 Absorption spectral features. The absorption peak energies of 2.22–2.61 eV are estimated for $AgInS_2$ NPs with the average diameters of 2.5–5.6 nm in this study. The bulk crystals of $AgInS_2$ with chalcopyrite and orthorhombic structures have direct band gaps with energies of 1.87 and 1.98 eV, respectively.[16] The observed peak energies are 0.2–0.7 eV larger than the bulk band gap values and exhibit the remarkable size-dependent blue-shift with decreasing NP size. A similar size-dependent shift is also observed in the PL spectra shown in Fig. 3. These observations strongly suggest a quantum confinement effect on carriers in these $AgInS_2$ NPs, as reported for many kinds of semiconductor NPs, including I-III-VI_2 NPs.[17] Therefore, we conclude that those absorption bands are due to the transition between the lowest quantized levels of the valence and conduction bands in $AgInS_2$ NPs.

4.2.2 PL mechanism. Metathesis-synthesized $AgInS_2$ NPs exhibit broad PL bands (FWHM ~0.4 eV) with large Stokes shifts (0.8–1.0 eV) from the lowest transition energy as shown in Fig. 3, suggesting that the PL originates in intra-gap levels, not in the transition between quantized energy levels in conduction and valence bands. The PL band exhibits the blue-shift with an increase of the excitation laser intensity (Fig. 4(a)). This observation is a characteristic phenomenon of pair-recombination of electrons and holes trapped by defect sites such as donors and acceptors, D–A pair recombination.[18] The excitation power dependence of the PL band for NPs with a diameter of 2.5 nm can be described by the power law ($I \propto L^k$) with $k = 0.97$ (Fig. 4(b)). According to Schmidt *et al.*, the exponent k is below 1 for free-to-bound and D–A pair recombination, while k is above 1 for excitonic emission.[10] Thus, the value of $k = 0.97$ is consistent with our tentative assignment that the PL of metathesis-synthesized $AgInS_2$ NPs is ascribed to the D–A pair recombination.

We have observed the characteristic behavior of PL decay time depending on the emission energies, where the effective decay time increases with a decrease in the emission energy (Fig. 5). Such a behavior also agrees with a characteristic property of the PL due to the D–A pair recombination. In a D–A pair emission process, the Coulombic interaction between donor and acceptor modifies their binding energies, hence the distant pairs have lower transition energies. The recombination probability between electrons and holes on close pairs is higher than that between the distant pairs, because of a larger overlap of their wavefunctions. Therefore, the recombination rate for a high-energy transition becomes high compared with that for a low-energy transition, resulting in shorter decay times for higher emission energies that are coincident with the PL decay behavior observed in this study. Similar variations of the decay time depending on the emission energies were observed in the PL of $CuInS_2$ and CdS NPs which are assigned to the D–A pair emission.[19,20] Consequently, the observations on the PL spectra and PL decay times indicate that the PL of the metathesis-synthesized $AgInS_2$ NPs is due to the D–A pair recombination. For the D–A pair emission in bulk semiconductors, the variation of the PL decay time amounts to two or three orders of magnitude.[18] The effective decay time measured in this study varies over an order of magnitude (60–760 ns), which is much smaller than the variation for bulk semiconductors. In NP systems, the distance between donors and acceptors is limited by the NP diameter, resulting in such a small variation of the decay time.

The broad spectral features observed in our $AgInS_2$ NPs originate mainly in emission mechanisms due to the D–A pair recombination, but the PL band may be slightly broadened due to the size distribution of NPs.

In bulk $AgInS_2$ crystals with chalcopyrite structures, intra-gap levels with donor- and acceptor-characters are created by several kinds of defects, such as vacancies and interstitial atoms, and PL bands with various energies are observed in addition to the band edge emission. These PL bands are interpreted as a free-to-bound transition and D–A pair recombination.[21] Former studies on chalcopyrite $AgInS_2$ thin films indicated that Ag vacancies and interstitial S atoms tend to create acceptor levels, while S vacancies and interstitial Ag atoms create donors.[21] Therefore, similar defects present in $AgInS_2$ NPs are probably related to the D–A pair PL. Additionally, defects on surfaces of nanoparticles may take an important role in D–A pair recombination processes.

Recently, broad emission bands similar to those observed in this study were reported for $CuInS_2$ NPs, and the main parts of the emission bands were assigned to the D–A pair transition.[19,22,23] The intrinsic defects, not the surface defects, were proposed as the trapping sites associated with the D–A pair transition.[22,23] However, previous studies on CdSe and CdS NPs provided experimental evidence that the emission bands with large Stokes shifts were due to the D–A pair recombination of electrons and holes trapped at the surface defects such as vacancies, dangling bonds, and oxygen adatoms.[20,24] Presumably, the same kinds of surface defects are present in $AgInS_2$ NPs and create the trapping sites for the D–A pair recombination. In accordance with this assumption, two PL decay times τ_A (shorter) and τ_B (longer) may be interpreted in terms of the D–A pair recombination of electrons and holes trapped in the intrinsic (core) defects, and the surface defects, respectively.

5. Summary

A $Ag/AgInS_2$ nanocomposite and $AgInS_2$ NPs with chalcopyrite-like and orthorhombic structures were successfully synthesized *via* thermolysis and sulfurization of metal–thiol complexes. Size tuning was conducted—very fine $AgInS_2$ NPs with a chalcopyrite structure could be obtained; the particle size could be tuned within 2.5–4.3 nm by changing reaction temperature. The PL peak of $AgInS_2$ NPs with an average size of 2.5 nm exhibits a marked Stokes shift at room temperature and its peak energy is about 1.6 eV. The excitation intensity dependence of the PL peak energy, and the wide variation in the PL decay times depending on the emission energy, suggest that the observed PL is attributed to the donor–acceptor recombination.

Acknowledgements

This work was supported by a grant from Nippon Oil Corporation, Grant in Aid for Young Scientists (B) 21760596 and Intellectual Cluster Project of Aichi-Nagoya Area given by the Ministry of Education, Science, Culture and Sports (MEXT), Japan. A part of this research was performed under the Nanotechnology Support Project in Central Japan financially supported by the Nanotechnology Network Project of the MEXT.

References

1 (*a*) S. G. Bailey and D. J. Flood, *Progr. Photovolt.: Res. Appl.*, 1998, **6**, 1–14; (*b*) H. W. Schock and R. Noufi, *Progr. Photovolt.: Res. Appl.*, 2000, **8**, 151–160; (*c*) H. W. Schock and K. Bogus, Development of CIS solar cells for space applications, in *Proceedings of the Second World Conference on Photovoltaic Energy*, ed. J. Schmid, H. A. Ossenbrink, P. Helm, H. Ehmann and E. D. Dunlop, EC Joint Research Center, Luxembourg, 1998, 3586–3589; (*d*) E. Arici, N. S. Sariciftci and D. Meisnner, *Adv. Funct. Mater.*, 2003, **13**, 165–171; (*e*) M. Nanu, J. Schoonman and A. Goossens, *Nano Lett.*, 2005, **5**, 1716–1719.
2 http://www.honda.co.jp/news/2008/c081023.html (Press release).
3 (*a*) Q. Guo, S. J. Kim, M. Kar, W. N. Shafarman, R. W. Birkmire, E. A. Stach, R. Agrawal and H. W. Hillhouse, *Nano Lett.*, 2008, **8**, 2982–2987; (*b*) M. G. Panthani, V. Akhavan, B. Goodfellow, J. P. Schmidtke, L. Dunn, A. Dodabalapur, P. F. Barbara and B. A. Korgel, *J. Am. Chem. Soc.*, 2008, **130**, 16770–16777.
4 (*a*) S. L. Castro, S. G. Bailey, R. P. Rafaelle, K. K. Banger and A. F. Hepp, *Chem. Mater.*, 2003, **15**, 3142–3147; (*b*) M. T. Ng, C. B. Boothroyd and J. J. Vittal, *J. Am. Chem. Soc.*, 2006, **128**, 7118–7119.
5 T. Torimoto, T. Adachi, K. Okazaki, M. Sakuraoka, T. Shibayama, B. Ohtani, A. Kudo and S. Kuwabata, *J. Am. Chem. Soc.*, 2007, **129**, 12388–12389.
6 (*a*) S. Choi, E. Kim and T. Hyeon, *J. Am. Chem. Soc.*, 2006, **128**, 2520–2521; (*b*) T. Kino, T. Kuzuya, K. Itoh, K. Sumiyama, T. Wakamatsu and M. Ichidate, *Mater. Trans.*, 2008, **49**, 435–438.
7 L. Tian, H. I. Elim, W. Ji and J. J. Vittal, *Chem. Commun.*, 2006, 4276–4278.
8 Y. Hamanaka, T. Kuzuya, T. Sofue, T. Kino, K. Itoh and K. Sumiyama, *Chem. Phys. Lett.*, 2008, **466**, 176–180.
9 E. Lippert, W. Nagele, I. Seibold-Blankenstein, U. Taiger and W. Voss, *Fresenius' Z. Anal. Chem.*, 1959, **170**, 1–18.
10 T. Schmidt, K. Lischka and W. Zulehner, *Phys. Rev. B: Condens. Matter*, 1992, **45**, 8989–8994.
11 T. H. Larsen, M. Sigman, A. Ghezelbash, R. C. Doty and B. A. Korgel, *J. Am. Chem. Soc.*, 2003, **125**, 5638–5639.
12 D. Wang, T. Xie, Q. Peng and Y. Li, *J. Am. Chem. Soc.*, 2008, **130**, 4016–4022.
13 T. Kuzuya, K. Itoh and K. Sumiyama, *J. Colloid Interface Sci.*, 2008, **319**, 565–571.
14 Japanese Patent Application No. 2007-135374; Japanese Published Unexamined Patent Application No. 2009–13019.
15 (*a*) W. Freyland, O. Madelung, U.Rossler and M. Schulz, *Landolt-Börnstein*, Group III, vol. 17e, 1983, 139–140; (*b*) W. Lou, X. Wang, M. Chen, W. Liu and J. Hao, *Nanotechnology*, 2008, **19**, 225607; S. P. Anthony, *Mater. Lett.*, 2009, **63**, 773–776; (*c*) M. Böhm and O. Madelung, "*Landolt-Börnstein*" Gr. III, Vol. 17h, 1985, Springer-Verlag, Berlin.
16 J. L. Shay and J. H. Wernick, *Ternary Chalcopyrite Semiconductors: Growth, Electronic Properties, and Applications*, Pergamon Press, Oxford, 1975.
17 *Nanostructured Materials and Nanotechnology*, ed. H. S. Nalwa, Academic Press, San Diego, 2000.
18 J. I. Pankove, *Optical processes in semiconductors*, Dover publications, New York, 1971.
19 H. Zhong, Y. Zhou, M. Ye, Y. He, J. Ye, C. He, C. Yang and Y. Li, *Chem. Mater.*, 2008, **20**, 6434–6443.
20 N. Chestnoy, T. D. Harris, R. Hull and L. E. Brus, *J. Phys. Chem.*, 1986, **90**, 3393–3399.
21 (*a*) M. L. Albor-Aguilera, J. R. Aguilar-Hernández, M. A. González -Trujillo, M. Ortega-López and G. Contreras-Puente, *Thin Solid Films*, 2007, **515**, 6272–6275; (*b*) S. H. You, K. J. Hong, C. J. Youn, T. S. Jeong, J. D. Moon, H. S. Kim and J. S. Park, *J. Appl. Phys.*, 2001, **90**, 3894–3898; (*c*) J. Krustok, J. Raudoja, M. Krunks, H. Mändar and H. Collan, *J. Appl. Phys.*, 2000, **88**, 205–209; (*d*) G. Massé and E. Redjai, *J. Appl. Phys.*, 1986, **59**, 1544–1547.
22 S. L. Castro, S. G. Bailey, R. P. Raffaelle, K. K. Banger and A. F. Hepp, *J. Phys. Chem. B*, 2004, **108**, 12429–12435.
23 H. Nakamura, W. Kato, M. Uehara, K. Nose, T. Omata, S. Otsuka-Yao-Matsuo, M. Miyazaki and H. Maeda, *Chem. Mater.*, 2006, **18**, 3330–3335.
24 E. Lifshitz, I. Dag, I. Litvin, G. Hodes, S. Gorer, R. Reisfeld, M. Zelner and H. Minti, *Chem. Phys. Lett.*, 1998, **288**, 188–196.